



POWER FLOW IN BEAMS TREATED WITH ACTIVE CONSTRAINED LAYER DAMPING

Abdulmalik Ali Aljinaidi Alghamdi¹ and Amr Baz²

1: Associate Professor, Department of Production Engineering and Mechanical Systems Design
P O Box 80251, King Abdulaziz University, Jeddah 21589, Saudi Arabia

E-mail: aljinaidi@hotmail.com (The Corresponding Author)

2: Professor, Department of Mechanical Engineering, University of Maryland at College Park
College Park, MD 20742, USA

ABSTRACT

This paper presents the power flow characteristics of beams treated with Active Constrained Layer Damping (ACLD). In the ACLD, a viscoelastic layer is sandwiched between two plies of active piezoelectric material. The presence of the ACLD in a vibrating structure reduces the vibration amplitude by dissipating the vibrational energy in shearing the viscoelastic layer. Numerical examples show the passive and active net power flow cantilever beams. The obtained results show the potential of the power flow analysis in modeling ACLD element and the merits of ACLD in controlling the power flow in structures.

Keywords: Active, Constrained, Layer, Damping, ACLD, Power, Flow, piezoelectric

ACLD .(ACLD)

ACLD

ACLD

ACLD

1. INTRODUCTION

Power flow analysis has been developed to study the dynamic response of structures for many years. Unlike statistical energy analysis, which predicts an overall structural response, power flow analysis enables the computation of the spatial variation of the dynamic response throughout the entire structure. Efforts made to use power flow in analysis of dynamic systems go back to the pioneering work of Nefske and Sung (1989). Since then, power flow techniques have been used to study the dynamic response of discrete systems [Alfredsson, 1997], rods [Wohlever and Bernhard, 1992], beams [Alfredsson, 1997; Wohlever and Bernhard, 1992; Pan and Hansen, 1991; Alfredsson et al., 1996], plates [Alfredsson, 1997; Hambric 1990; Zhou and Rogers, 1995], simple trusses [Hambric 1990] and shells [Alfredsson et al., 1996]. Experiments on power flow have been carried out for one-dimensional structures in the form of cantilever beams [Gibbs and Fuller 1992; Gibbs et al., 1993] and thin plates [Zhou and Rogers, 1995].

In this paper, the power flow analysis is extended to study the dynamic response of beams treated with the new class of Active Constrained Layer Damping (ACLD) treatment. The ACLD has attracted significant attention in the past few years as it provides an effective means for attenuating structural vibrations. In the ACLD, a composite patch made of piezoelectric sensor, viscoelastic material (VEM) and actuator is bonded to the surface of the structure. In its open-loop mode of operation, the VEM undergoes shear strain resulting in dissipating energy and hence damping out the structural vibration, as shown in Figure 1. If the sensor voltage V_s is amplified and sent to the actuator, the VEM is exposed to an additional shear strain and more energy is dissipated.

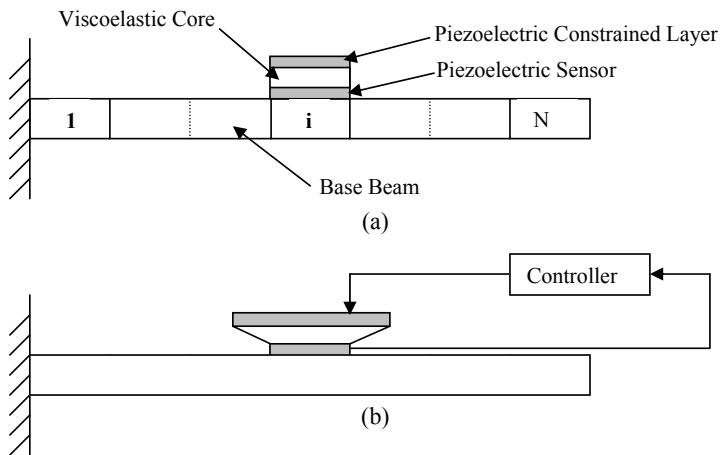


Figure 1: Schematic drawing of the ACLD treatment: a. Open-loop, b. Closed-loop.

The concept of ACLD has been successfully used to control the vibration in beams [Baz, 1993; Baz and Ro, 1994; Baz and Ro, 1995; Shen 1995; Huang et al., 1996], plates [Baz and Ro, 1996b; Veley and Rao, 1996; Holkamp and Gordon, 1996], shells [Baz and Chen, 1997] and rings [Rongong and Tomlinson, 1996]. The ACLD has also been utilized in attenuating noise radiation into acoustic cavities [Poh et al., 1996]. Investigators [Baz and Ro, 1995b; Ro and Baz, 1996; Baz and Ro, 1996a] have carried out optimum design and control of beams treated with ACLD. Lesieutre and Lee [1996] developed finite element for beams with continuous or segmented ACLD treatments. Liao and Wang [1996] proposed hybrid active-passive constrained treatment for beams. Yellin and Shen [1996] presented a self-sensing controller for beams with ACLD treatment.

2. POWER FLOW IN STRUCTURES

Power flow displays how the mechanical energy is transported within the structure as it flows from the excitation source until it is dissipated at the energy sinks [Alfredsson, 1997]. Nefske and Sung [1989] developed the power flow analysis for high-frequency response of beams using formulation adaptable to finite element analysis. Their formulation was based on conservation of the energy over a controlled volume. Energy flow within each subsystem was predicted. In 1990, Hambric identified the power flow and mechanical intensities in finite element models for plates and trusses. Different types of power flow waves including, flexural, axial, and torsional, were discussed. Power flow in simple truss and beam-stiffened cantilever plate was examined. Wohlever and Bernhard [1992] studied energy flow in longitudinal vibration in rods and transverse flexural vibrations of beams. Power density equations were derived from the displacement solutions for harmonically excited coupled and free rods and beams. Active control of the flexural power flow in vibrating beams was experimentally investigated by Gibbs and Fuller [1992]. In their setup, an axial scanning laser vibrometer is used to determine the out-of-plane velocity, which is used to predict the power flow along the beam. Net power flow is calculated using cross spectrum of the velocity response. The sensor signal is sent to an adaptive least mean squares narrow-band controller. The output of the controller is used to derive two actuators in the form of piezoceramic transducer bonded symmetrically on each side of the beam. The obtained results for harmonically excited beam show 30-dB reduction in the net power flow along the beam. The study illustrated the potential of piezoceramic elements in power flow control. A model for analyzing the power flow in transverse, shear, and longitudinal waves, resulted from primary excitation and control forces was given by Pan and Hansen [1991]. The model is based on the classical beam theory for infinitely long beams. The study concludes that effective control of the power flow requires an independent control force for each wave. Gibbs et al. [1993] presented a method to estimate the extensional and flexural power flow in the time domain using piezoelectric surface bonded element and a digital filter network. The method was verified experimentally and attenuation of flexural power flow over 40 dB, for a narrow band disturbance, was achieved. Zhou and Rogers [1995] investigated the power flow in piezoelectrically actuated plates using a coupled electromechanical system model. The study

shows that the energy supplied by the piezoelectric actuators is consumed by the structural damping of the host structure at resonant frequencies. The thickness and location of the actuator have a major role in dissipating energy because of the change in the mechanical impedance of the structure. Alfredsson et al. [1995] uses the energy flow concept in designing a vibrating system. Energy flow is calculated using harmonic response finite element analyses. The study includes two examples, one for a frame made of Euler-Bernoulli beam elements and the other for shell structure. In another paper, Alfredsson [1997] presented the details of active and reactive (stored) energy flow in structures. Numerical examples with discrete, continuous and discretized structures were given.

Consider an elastic solid subjected to time-varying external loads. The energy continuity equation is given by [Alfredsson, 1997],

$$\dot{W} + \Pi = L - q_{i,i} \tag{1}$$

The term \dot{W} is the power being stored in the solid, which is the sum of the strain and kinetic powers, Π is the net power flow inside the structure, L is the power supplied per unit volume by external body forces, and $q_{i,i}$ is the power supplied through boundaries. For stationary harmonic vibration at given frequency, ω , the complex mechanical intensity c_i is introduced as,

$$c_i = a_i + i r_i \tag{2}$$

The real part a_i is the active mechanical intensity defined as the net energy flow rate per unit cross-sectional area. The imaginary part r_i is the reactive mechanical intensity, and i is the imaginary units. The continuity equation for the active and reactive intensities may be written as [Alfredsson, 1997],

$$a_{i,i} = P - \Pi \tag{3}$$

$$r_{i,i} = Q - 2\omega(U - T) \tag{4}$$

Quantities P , Q , U , and T are the supplied active power, the supplied reactive power, the elastic strain energy density, and the kinetic energy density, respectively. Balance between supplied power, consumed and stored powers gives zero divergences of the active and reactive mechanical intensity vector fields. Thus,

$$P = \Pi \tag{5}$$

and

$$Q = 2\omega(U - T) \tag{6}$$

Here the supplied active power is equal to the net power flow in the structure, and the supplied reactive power is related to the difference between the strain and the kinetic energies. For a discrete structure modeled using finite element method, the equation of motion is given as

$$\mathbf{M} \ddot{\underline{\mathbf{X}}} + \underline{\mathbf{K}} \underline{\mathbf{X}} = \mathbf{F} \quad (7)$$

Matrices \mathbf{M} and $\underline{\mathbf{K}}$ are the mass and complex stiffness matrices, respectively, with the underline denoting a complex variable. The vector $\underline{\mathbf{X}}$ is the nodal degrees of freedom (DOF). For beam element, the nodal DOF include the lateral displacement and rotation. In addition to this, the ACLD has two more DOF in the longitudinal direction, as outlined in Section 3. The force vector \mathbf{F} includes both the external disturbance forces and the control forces. For linear system in stationary harmonic vibration, equation (7) is solved using matrix inversion,

$$\underline{\mathbf{X}} = \underline{\mathbf{e}} \mathbf{F} \quad (8)$$

where the matrix $\underline{\mathbf{e}}$ is given by

$$\underline{\mathbf{e}} = (\underline{\mathbf{K}} - \omega^2 \mathbf{M})^{-1} \quad (9)$$

The net power flow as well as the strain and kinetic energies are given as,

$$\Pi = \frac{1}{2} \dot{\underline{\mathbf{X}}}^H \mathbf{C} \dot{\underline{\mathbf{X}}} \quad (10)$$

$$\mathbf{U} = \frac{1}{4} \underline{\mathbf{X}}^H \underline{\mathbf{K}} \underline{\mathbf{X}} \quad (11)$$

$$\mathbf{T} = \frac{1}{4} \dot{\underline{\mathbf{X}}}^H \mathbf{M} \dot{\underline{\mathbf{X}}} \quad (12)$$

Dot and H superscript denotes time derivative and Hermitian transpose, respectively. Matrix \mathbf{C} is imaginary part of the complex stiffness matrix $\underline{\mathbf{K}}$.

3. ACTIVE CONSTRAINED LAYER DAMPING (ACLD)

In the ACLD, a viscoelastic layer is sandwiched between two piezoelectric films, which are bonded to the vibrating structure. One of the piezo-films acts as a sensor while the other acts as an actuator. The output voltage of the sensor is conditioned and sent back to the actuator inducing strain in the actuator as shown in Figure 1. As a result, the viscoelastic material is subjected to high shear strain and hence dissipates more energy.

The ACLD concept was successfully utilized to control the vibration of beams, plates and shells using simple analog controllers. Baz and Ro [1995a] presented a finite element model of beams that are partially treated with ACLD. The predictions of the model were verified experimentally and the experimental performance of the ACLD was compared with that of the passive constrained layer damping. Optimum design and control of beams was studied by Baz and Ro [1995b]. Optimum thickness and shear modulus of the viscoelastic material were determined based on maximizing the modal damping ratio and minimizing the weight of the

ACLD. Optimal velocity feedback controller of the ACLD was found to be more effective than PCLD controller by two orders of magnitudes. In another paper, Ro and Baz [1996] investigated the optimum design and control of beams with segmented configuration of ACLD. The thickness, length, and shear modulus of the viscoelastic material were determined. Baz and Ro [1996a] compared the characteristics of beams controlled with Active Control (AC), ACLD and PCLD. The obtained results demonstrate high damping characteristics of the ACLD with low control voltage. Similar finite element models and experimental performance characteristics are developed for vibration control of plates [Baz and Ro, 1996b] and shells [Ray et al., 1997] treated with discrete ACLD patches.

Figure 1 shows schematic drawing of a partial ACLD treatment for a cantilever beam which is divided into N elements. The shear strain in the base beam is neglected and the transverse displacement at any cross section along the composite beam is assumed constant. Core material is assumed to be linearly viscoelastic. Also, perfect bonding conditions are assumed everywhere, thus, the sensor and the beam are treated as single sensor/base beam layer. The shear strain in of the viscoelastic core is given by [Baz and Ro, 1995a],

$$\gamma = [hw_x + (u_1 - u_3)]/h_2 \tag{13}$$

Where

$$h = h_2 + h_1/2 + h_3/2 \tag{14}$$

With h_1 , h_2 and h_3 denoting the thickness of the actuator, the viscoelastic core and sensor/beam layer, respectively. Functions u_1 and u_3 are the longitudinal displacements of the piezoelectric actuator and the beam/sensor layer, respectively. The spatial distributions of the longitudinal displacements u_1 and u_3 and the transverse deflection w over element i are assumed to be,

$$u_1 = a_1 x + a_2, \quad u_3 = a_3 x + a_4 \tag{15}$$

$$w = a_5 x^3 + a_6 x^2 + a_7 x + a_8 \tag{16}$$

Constants a_i are determined in terms of the eight components of the nodal deflection vector $\{\Delta_i\}$ of the i th element which is bounded between nodes j and k . The nodal deflection vector is given by,

$$\{\Delta_i\} = \{u_{1j}, u_{3j}, w_j, w'_j, u_{1k}, u_{3k}, w_k, w'_k\}^T \tag{17}$$

With primes denoting spatial derivatives. The deflection $\{\Delta_i\}$ at any location x along the i th element can be written as,

$$\{u_1, u_3, w, w'\}^T = \{[N_1], [N_2], [N_3], [N_4]\}^T \{\Delta_i\} \tag{18}$$

Where $[\mathbf{N}_1]$, $[\mathbf{N}_2]$, $[\mathbf{N}_3]$, and $[\mathbf{N}_4]$ are the spatial interpolating vectors corresponding to u_1 , u_2 , w , and w' respectively. For ACLD-treated beam element the equation of motion, given by equation (7), is described by the following equation,

$$[\mathbf{M}_i]\{\ddot{\Delta}_i\} + [\mathbf{K}_i]\{\Delta_i\} = \{\mathbf{F}_c\} \quad (19)$$

Where $[\mathbf{M}_i]$ and $[\mathbf{K}_i]$ are the stiffness and mass matrices of the i th beam element given in Appendix A. The control force $\{\mathbf{F}_c\}$ is given by [Baz and Ro, 1995b],

$$\{\mathbf{F}_c\} = \{\mathbf{F}_{pj}, 0, 0, \mathbf{M}_{pj}, \mathbf{F}_{pk}, 0, 0, \mathbf{M}_{pk}\}^T \quad (20)$$

Elements of $\{\mathbf{F}_c\}$ are also given in the Appendix B.

4. NUMERICAL EXAMPLES

In this section, numerical examples are given for beams fully treated with the ACLD. The theoretical net power flow is given for different excitation frequencies. Figure 1 represents a schematic drawing of the beam treated with one ACLD. In this section, a cantilever beam made of steel is used as a base beam. The constrained layer is made of piezoceramic (PZT-1195) and the viscoelastic material is DYAD-606. The physical properties of these materials are shown in Tables 1 and 2. It is assumed that the physical properties are independent of the frequency and temperature. The complex shear modulus of the VEM is assumed to be,

$$G = 20 \times 10^6 (1 + i) \quad (21)$$

The first three natural frequencies of the uncontrolled fully treated beam made of 32 elements are 54 Hz, 335 Hz and 937 Hz, respectively.

Figure 2 shows the frequency response function of the beam when it is fully covered with the ACLD and subjected to unit end transverse load. The beam is divided into 32 equally spaced elements. The solid line gives the passive response of the beam when it operates in its open-loop mode. The dashed line depicts the active closed-loop response using a velocity feedback gain $K_d=50$. As shown in the figure, considerable attenuation of the first three modes was achieved using small feedback gain.

Table 1: Physical Properties of the Base Beam and the Viscoelastic Materials.

Material	Length (m)	Thickness (m)	Width (m)	Density (Kg/m ³)	Young's Modulus (MPa)
Steel	0.5	0.0125	0.05	7800	210 000
VEM (DYAD-606)	0.5	0.00625	0.05	1104	60

Table 2: Physical Properties of the Piezoelectric Constraining Layer.

Length (m)	Thickness (m)	Width (m)	Density (Kg/m ³)	Young's Modulus (GPa)	d31 (m/V)	K31	g31 (Vm/N)	k3t
0.5	0.0025	0.05	7600	63	186e-12	0.34	116e-2	1950

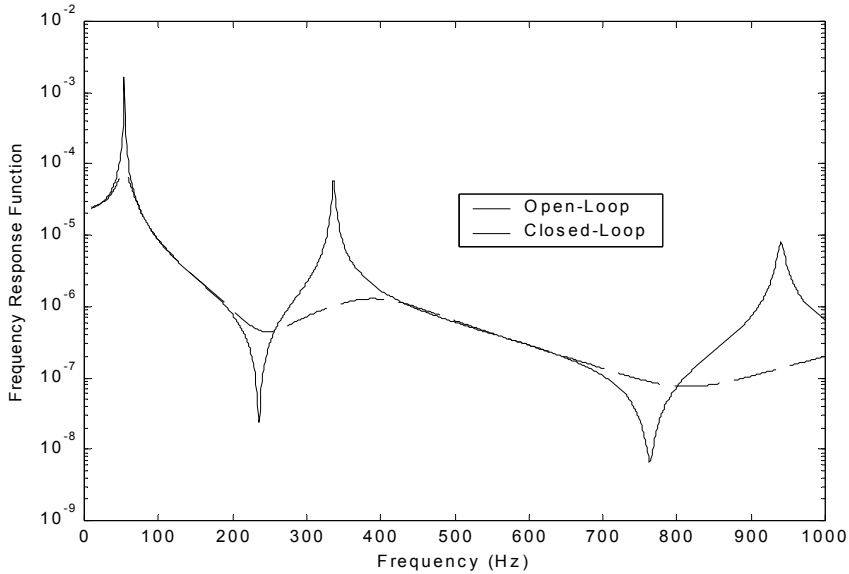


Figure 2: Open and closed-loop frequency response functions of fully treated beam.

5. RESULTS AND DISCUSSIONS

Figure 3 shows the net power flow of the fully treated beam versus the excitation frequency. The passive response shows that net power flow attains a maximum at the resonant frequencies. The dashed line illustrates the active response corresponding to $K_d = 50$. Hence, the net power flow is considerably reduced as the feedback gain is increased from zero to 50. Such reduction is attributed to the attenuation of the beam vibration.

The net power flow, along the beam, is shown in Figure 4 for three different excitation frequencies (54 Hz, 335 Hz and 937 Hz) which correspond to the first three natural frequencies of the beam/ACLD composite. Figure 4 shows also comparisons between the open-loop ($K_d = 0.0$) and closed-loop ($K_d = 5$) characteristics. It is that the spatial profile of the net power flow at any particular natural frequency is similar to the corresponding mode shape of the beam. Also, note that there is a significant attenuation of the net power flow due to the activation of the ACLD controller even though $K_d = 5$.

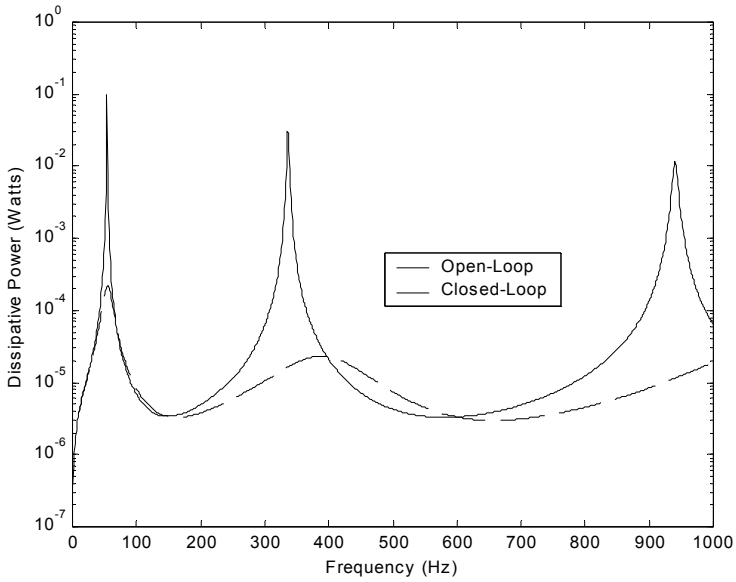


Figure 3: Open and closed-loop net power flow of fully treated beam.

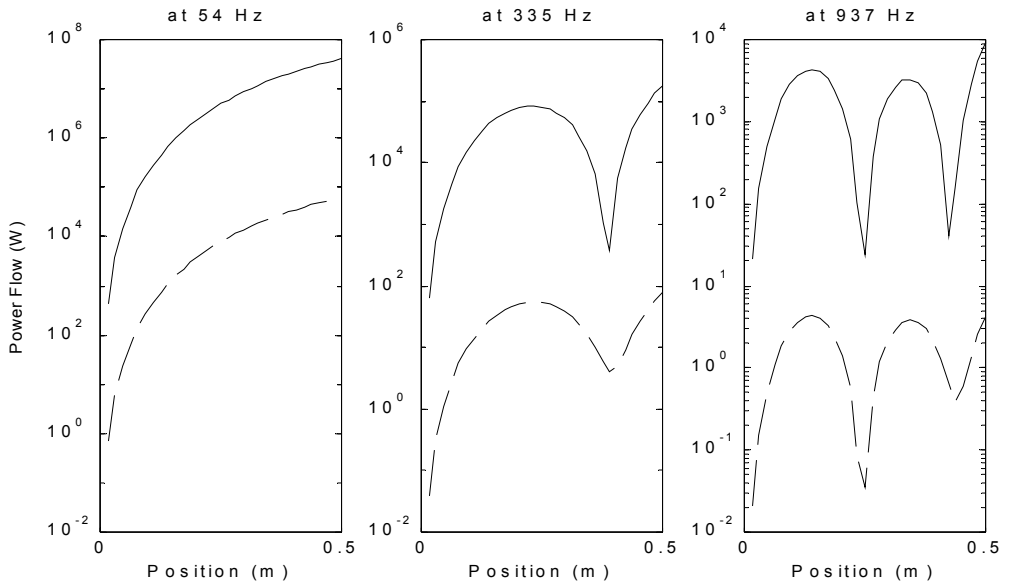


Figure 4: Net power flow versus the beam position for fully treated beam.

a. 54 Hz, b. 335 Hz, c. 937 Hz.

6. CONCLUSIONS

This paper has presented an analysis of the power flow in beams treated with Active Constrained Layer Damping (ACLD) treatments. The power flow method is utilized to provide quantitative means for the behavior of beam with patches of the ACLD treatment. The power flow method is summarized first and the mechanics of active constrained layer treatment is outlined. Numerical examples are presented to illustrate the net power flow characteristics in beams/ACLD systems both in the frequency and the spatial domains. It is evident that the active constrained layer treatment reduces considerably the net power flow in beams.

7. ACKNOWLEDGEMENT

This research is funded by the US Army through their University Research Initiative, Dr. Gary Anderson is the technical monitor. The first author would like also to thank King Abdulaziz University, Jeddah, Saudi Arabia for supporting this research through his sabbatical leave during 2001/2002 academic year.

REFERENCES

1. Alfredsson, K. S., 1997, "Active and Reactive Structural Energy Flow," *Journal of Vibration and Acoustics*, 119, pp. 70-79.
2. Alfredsson, K. S., Josefon, B. L. and Wislon, M. A., 1996, "Use of the Energy Flow Concept in Vibration Design," *AIAA Journal*, 34, pp. 1250-1255.
3. Baz, A., 1993, "Active Constrained Layer Damping," *DAMPING'93 Conference*, San Francisco, CA, 3, pp. 1-23.
4. Baz, A. and Chen, T., 1997, "Boundary Control of Axisymmetrical Vibration of Cylindrical Shells Using Active Constrained Layer Damping," *Proceedings Of AIAA Aerospace Sciences Conference*, Symposium on Non-Linear Dynamic Systems, Reno, Nevada, pp. 168-180.
5. Baz, A. and Ro, J., 1994, "The Concept and Performance of Active Constrained Layer Damping Treatments," *Sound and Vibration Magazine*, 20, pp. 18-21.
6. Baz, A. and Ro, J., 1995a, "Performance Characteristics of Active Constrained Layer Damping," *Shock and Vibration Journal*, 2, pp. 33-42.
7. Baz, A. and Ro, J., 1995b, "Optimum Design and Control of Active Constrained Layer Damping," *Journal of Vibration and Acoustics*, 117, pp.135-144.
8. Baz, A. and Ro, J., 1996a, "Active Control and Passive Constrained Layer Damping Versus Active Constrained Layer Damping," *Journal of Vibration and Control*, Submitted.
9. Baz, A. and Ro, J., 1996b, "Vibration Control of Plates with Active Constrained Layer Damping," *Smart Materials and Structures*, 5, pp. 272-280.
10. Gibbs, G. P. and Fuller, C. R., 1992, "Experiments on Active Control of Vibrational Power Flow Using Piezoceramic Actuator/Sensor," *AIAA Journal*, 30, pp. 457-463.

11. Gibbs, G. P., Fuller, C. R. and Silcox, R. J., 1993, "Active Control of Flexural and Extensional Power Flow in Beams Using Real Time Wave Vector Sensors," *Second Conference on Recent Advances in Active Control of Sound and Vibration*, VPI and State University, pp. 909-925.
12. Hambric, S. A., 1990, "Power Flow and Mechanical Intensity Calculations in Structural Finite Element Analysis," *Journal of Vibration and Acoustics*, 112, pp. 542-549.
13. Holkamp, J. J. and Gordon, R. W., 1996, "An Experimental Comparison of Piezoelectric and Constrained Layer Damping," *Smart Materials and Structures*, 5, pp. 715-722.
14. Huang, S. C., Inman, F. J. and Austin, E. M., 1996, "Some Design Considerations for Active and Passive Constrained Layer Damping Treatments," *Smart Materials and Structures*, 5, pp. 301-313.
15. Lesieutre, G. A. and Lee, U. 1996, "A Finite Element for Beams Having Segmented Active Constrained Layers with Frequency-Dependent Viscoelastics," *Smart Materials and Structures*, 5, pp. 615-627.
16. Liao, W. H. and Wang, K. W., 1996, "A New Active Constrained Layer Configuration with Enhanced Boundary Actions," *Smart Materials and Structures*, 5, pp. 638-648.
17. Nefske, O. J. and Sung, S. H., 1989, "Power Flow Finite Element Analysis of Dynamic Systems: Basic Theory and Application to Beams," *Journal of Vibration and Acoustics*, 111, pp. 94-100.
18. Pan, J. and Hansen, C., 1991, "Active Control of Total Vibratory Power in a Beam. I: Physical System Analysis," *Journal of Acoustic Society of America*, 89, pp. 200-209.
19. Poh, S., Baz, A. and Balachandran, B., 1996, "Experimental Adaptive Control of Sound Radiation from a Panel Into an Acoustic Cavity Using Active Constrained Layer Damping," *Smart Materials and Structures*, 5, pp. 649-659.
20. Ray, M., Chen, T. and Baz, A., 1997, "Vibration Control of Cylindrical Shells Using Active Constrained Layer Damping," *Smart Structures and Material Conference*, San Diego, CA, pp. 293-314.
21. Ro, J. and Baz, A., 1996, "Optimum Design and Control of Partial Active Constrained Layer Damping Treatments," *Journal of Vibration and Control*, Submitted.
22. Rongong, J. A. and Tomlinson, G. R., 1996, "Suppression of Ring Vibration Modes of High Nodal Diameter Using Constrained Layer Damping Methods," *Smart Materials and Structures*, 5, pp. 672-648.
23. Shen, I. Y., 1995, "Bending and Torsional Vibration Control of Composite Beams Through Intelligent Constrained-Layer Damping," *Smart Materials and Structures*, 4, pp. 340-355.
24. Velej, D. E. and Rao, S. S., 1996, "A comparison of Active, Passive and Hybrid Damping in Structural Design," *Smart Materials and Structures*, 5, pp. 660-671.
25. Wohlever, J. C. and Bernhard, R. J., 1992, "Mechanical Energy Flow Models of Rods and Beams," *Journal of Sound and Vibration*, 153, pp.1-19.
26. Yellin, J. M. and Shen, I. Y., 1996, "A Self-Sensing Active Constrained Layer Damping Treatment for an Euler-Bernoulli Beam," *Smart Materials and Structures*, 5, pp. 628-637.
27. Zhou, S-W. and Rogers, C., 1995, "Power Flow and Consumption in Piezoelectrically Actuated Structures," *AIAA Journal*, 33, pp. 1305-1311.

APPENDIX A

STIFFNESS AND MASS MATRICES FOR THE ACLD ELEMENT

A.1. STRAIN ENERGIES AND STIFFNESS MATRIX

The strain energies associated with the various layers of the ACLD treatment are determined as follows:

a. constraining layer: The energies include:

$$\textit{Extension} \quad U_1 = \frac{1}{2} E_1 A_1 \{\Delta_i\}^T \left[\int_{L_i} [N_1']^T [N_1'] dx \right] \{\Delta_i\} \quad (A-1)$$

where E_1 and A_1 are the modulus of elasticity and area of cross section of the constraining layer.

$$\textit{Bending} \quad U_2 = \frac{1}{2} E_1 I_1 \{\Delta_i\}^T \left[\int_{L_i} [N_3'']^T [N_3''] dx \right] \{\Delta_i\} \quad (A-2)$$

where $E_1 I_1$ is the flexural rigidity of the constraining layer.

b. visco-elastic layer: The energies include

$$\textit{Extension} \quad U_3 = \frac{1}{2} E_2 A_2 \{\Delta_i\}^T \left[\int_{L_i} [N_5]^T [N_5] dx \right] \{\Delta_i\} \quad (A-3)$$

where E_2 and A_2 are the modulus of elasticity and area of cross section of the visco-elastic layer. Also $[N_5]$ is an interpolating matrix = $([N_1'] + [N_2'] + (h_1/2 - h_3) [N_3''])/2$.

$$\textit{Bending} \quad U_4 = \frac{1}{2} E_2 I_2 \{\Delta_i\}^T \left[\int_{L_i} [N_6]^T [N_6] dx \right] \{\Delta_i\} \quad (A-4)$$

where $E_2 I_2$ is the flexural rigidity of the visco-elastic layer and $[N_6]$ is an interpolating matrix = $([N_1'] - [N_2'] + (h_1/2 + h_3) [N_3''])/h_2$.

$$\textit{Shearing} \quad U_5 = \frac{1}{2} G_2 A_2 \{\Delta_i\}^T \left[\int_{L_i} [N_7]^T [N_7] dx \right] \{\Delta_i\} \quad (A-5)$$

where G_2 is the shear modulus of the visco-elastic layer. Also $[N_7]$ is an interpolating matrix = $([N_1'] - [N_2'] + h [N_3'']) / h_2$

c. sensor/beam layer: The energies include

$$\underline{\text{Extension}} \quad U_6 = \frac{1}{2} E_3 A_3 \{\Delta_i\}^T \left[\int_{L_i} [\mathbf{N}_2]^T [\mathbf{N}_2] dx \right] \{\Delta_i\} \quad (\text{A-6})$$

where E_3 and A_3 are the modulus of elasticity and area of cross section of the sensor/beam layer.

$$\underline{\text{Bending}} \quad U_7 = \frac{1}{2} E_3 I_3 \{\Delta_i\}^T \left[\int_{L_i} [\mathbf{N}_3]''^T [\mathbf{N}_3]'' dx \right] \{\Delta_i\} \quad (\text{A-7})$$

where $E_3 I_3$ is the flexural rigidity of the sensor/beam layer.

From equations (A-1) through (A-7), the total strain energy U can be written as:

$$U = \sum_{i=1}^7 U_i = \frac{1}{2} \{\Delta_i\}^T [\mathbf{K}_i] \{\Delta_i\} \quad (\text{A-8})$$

where $[\mathbf{K}_i]$ is the equivalent stiffness matrix of the i th element.

A.2. KINETIC ENERGIES AND MASS MATRIX

a. constraining layer: It is given by:

$$\begin{aligned} T_1 &= \frac{1}{2} \rho_1 A_1 \int_{L_i} (\dot{w}^2 + \dot{u}_1^2) dx \\ &= \frac{1}{2} \rho_1 A_1 \{\dot{\Delta}_i\}^T \left[\int_{L_i} ([\mathbf{N}_3]^T [\mathbf{N}_3] + [\mathbf{N}_1]^T [\mathbf{N}_1]) dx \right] \{\dot{\Delta}_i\} \end{aligned} \quad (\text{A-9})$$

where ρ_1 is the density of the constraining layer.

b. visco-elastic layer: It is given by:

$$T_2 = \frac{1}{2} \rho_2 A_2 \int_{L_i} (\dot{w}^2 + \dot{u}_2^2) dx = \frac{1}{2} \rho_2 A_2 \{\dot{\Delta}_i\}^T \left[\int_{L_i} ([\mathbf{N}_3]^T [\mathbf{N}_3] + [\mathbf{N}_8]^T [\mathbf{N}_8]) dx \right] \{\dot{\Delta}_i\} \quad (\text{A-10})$$

where ρ_2 is the density of the visco-elastic layer and $[\mathbf{N}_8] = ([\mathbf{N}_1] + [\mathbf{N}_2] + (h_1/2 - h_3)[\mathbf{N}_3'])/2$.

c. sensor/beam layer: It is given by:

$$T_3 = \frac{1}{2} \rho_3 A_3 \int_{L_i} (\dot{w}^2 + \dot{u}_3^2) dx = \frac{1}{2} \rho_3 A_3 \{\dot{\Delta}_i\}^T \left[\int_{L_i} ([N_3]^T [N_3] + [N_2]^T [N_2]) dx \right] \{\dot{\Delta}_i\} \tag{A-11}$$

where ρ_3 is the density of the sensor/beam layer.

From equations (A-9) through (A-11), the total kinetic energy T can be written as:

$$T = \sum_{i=1}^3 T_i = \frac{1}{2} \{\dot{\Delta}_i\}^T [M_i] \{\dot{\Delta}_i\} \tag{A-12}$$

where $[M_i]$ is the equivalent mass matrix of the *i*th element.

APPENDIX B

CONTROL FORCES AND MOMENTS GENERATED BY THE ACTIVE CONSTRAINING LAYER

B.1. WORK DONE BY THE PIEZO-ELECTRIC FORCES

The work done W_1 by the piezo-electric forces F_{pj} ($= - F_{pk}$) during to the extension of the piezo-electric constraining layer is given by:

$$W_1 = \frac{1}{2} E_1 A_1 \int_{L_i} \epsilon_c \epsilon_p dx \tag{B-1}$$

where ϵ_c and ϵ_p denote the longitudinal strain of the constraining layer and the strain induced by the piezo-electric effect respectively. These strains are given by:

$$\epsilon_c = \frac{\partial u_1}{\partial x} \quad \text{and} \quad \epsilon_p = \frac{d_{31}}{h_1} V_c \tag{B-2}$$

where d_{31} is the piezo-electric strain constant resulting from the application of the voltage V_c across the piezo-actuator layer. In equation (B-2), V_c is assumed constant over the length of the beam element. The voltage V_c is generated by applying a proportional and derivative control law to the piezo-sensor voltage V_s as follows:

$$V_c = -K_p V_s - K_d dV_s/dt \tag{B-3}$$

where K_p and K_d are the proportional and derivative control gains respectively. In equation (B-3) V_s is obtained form:

$$V_s = \frac{-k_{31}^2 D_d b}{g_{31} C} \sum_{i=i_s}^{i_f} \int_{L_i} f(x) \frac{\partial^2 w}{\partial x^2} dx \tag{B-4}$$

where D_d is the distance from the beam neutral axis to the sensor surface and $f(x)$ is a distribution shape function of the sensor ($f(x) = 1$ for uniform sensor). In equation (B-4), the sensor is extended between elements i_s and i_f . Also, k_{31} is the electro-mechanical coupling factor, g_{31} is the piezo-electric voltage constant and C is the capacitance of the sensor which is given by:

$$C = 8.854 \times 10^{-12} A k_{3t} / h_1 \tag{B-5}$$

here A is the sensor surface area and k_{3t} is the dielectric constant.

Combining equations (B-1) through (B-5) gives:

$$\begin{aligned} W_1 &= \frac{g}{2} (K_p + K_d p) \int_{L_i} f(x) \frac{\partial u_1}{\partial x} \frac{\partial^2 w}{\partial x^2} dx \\ &= \{\Delta_i\}^T \{F_p\} \end{aligned} \tag{B-6}$$

where $g = [E_1 b^2 d_{31}] [k_{31}^2 D_d / g_{31} C]$ (B-7)

and $\{F_p\} = [F_{pj} \quad 0 \quad 0 \quad 0 \quad F_{pk} \quad 0 \quad 0 \quad 0]^T$ (B-8)

with $F_{pj} = -F_{pk} = (K_p + K_d p) [0 \quad 0 \quad 0 \quad g / 2 \quad 0 \quad 0 \quad 0 \quad -g / 2] \{\Delta_i\}$ (B-9)

Equation (B-9) indicates that the piezo-electric control forces F_{pj} and F_{pk} are linear functions of the nodal deflection vector $\{\Delta_i\}$. Also, these forces depend on the parameter g which is defined in terms of the control gains and properties of the piezo-sensor and actuator as shown by equation (B-7).

B.2. WORK DONE BY THE PIEZO-ELECTRIC MOMENTS

The work done W_2 by the piezo-electric forces M_{pj} ($= -M_{pk}$) during to the bending of the piezo-electric constraining layer is given by:

$$\begin{aligned}
 W_2 &= \frac{E_1 A_1}{2} \int_{L_i} d\epsilon_p \frac{\partial^2 w}{\partial x^2} dx = \frac{g h}{2} (K_p + K_{dP}) \int_{L_i} f(x) \left(\frac{\partial^2 w}{\partial x^2} \right)^2 dx \\
 &= \{\Delta_i\}^T \{\mathbf{M}_p\}
 \end{aligned}
 \tag{B-10}$$

where
$$\{\mathbf{M}_p\} = [0 \ 0 \ 0 \ M_{pj} \ 0 \ 0 \ 0 \ M_{pk}]^T
 \tag{B-11}$$

with
$$M_{pj} = -M_{pk} = (K_p + K_{dP}) [0 \ 0 \ 0 \ g h \ g/2 \ 0 \ 0 \ -g h] \{\Delta_i\}
 \tag{B-12}$$

Equation (B-12) indicates also that the piezo-electric control moments M_{pj} and M_{pk} are linear functions of the nodal deflection vector $\{\Delta_i\}$. Also, these forces depend on the parameter g which is defined in terms